A PLASMA PRISM MODEL FOR AN ANOMALOUS DISPERSION EVENT IN THE CRAB PULSAR

D. C. Backer, T. Wong, & J. Valanju

Astronomy Department & Radio Astronomy Laboratory, University of California, Berkeley, CA
email: dbacker@astro.berkeley.edu

ABSTRACT

In 1997 October daily monitoring observations of the Crab pulsar at 327 MHz and 610 MHz with an 85ft telescope in Green Bank, WV showed a jump in the dispersion measure by 0.1 cm^{-3} pc. Pulses were seen simultaneously at both old and new dispersions over the course of several days. During the dispersion jump the pulsed flux diminished by an order of magnitude. In the months before this event the average pulse profiles contained faint "ghost" pulse components offset in phase from the regular main pulse and interpulse components by a nearly frequency independent time delay that quadratically diminished to zero over a month. After the dispersion event there was an order of magnitude increase in the level of scattering, as measured by pulse broadening at 327 MHz. There was also a curious shift in the rotational phase, a slowing down, at both frequencies at the time of the dispersion jump which we associate with intrinsic timing noise. All of the observed phenomena except this slowing down can be explained by the variable perturbing optics of a triangular plasma prism that is located in the filamentary interface between the synchrotron nebula and the supernova ejecta and which crosses the line of sight over a period of months. The required density, scale length and velocity are reasonable given previous observations and analysis of these filaments. Our study thus provides a probe of the plasma column on scales of 30 microarcsecond to 3 milliarcsecond (10^{12-14} cm) which complements scales accessible to optical emission line studies with HST resolution (10^{16-18} cm). In combination both observations provide a detailed look at a sample of the interface region that can be matched statistically to the results of numerical simulations.

Subject headings: Crab nebula, pulsars, supernova remnants, turbulence, scattering

1. INTRODUCTION

Observations of pulsar signals at multiple frequencies allow measurements of a number of properties of the intervening plasma. The quadratic dependence of arrival times on radio frequency yields the column density of electrons, or dispersion measure, along the path. At low frequencies pulses are broadened by multipath propagation (diffraction) effects owing to the presence of phase perturbations on transverse scales smaller than the Fresnel radius. These perturbations are the result of microscale electron density fluctuations. When the perturbations are confined to a small region along the sight line and have a wide extent transverse to the path, the broadening function is exponential. Phase pertubations that are large with respect to the Fresnel radius lead to refractive changes both in the path direction and in the signal amplitude. Most intervening media are birefringent, and as a result the reference angle of linear polarization undergoes Faraday rotation as a function of radio frequency. Temporal changes in all of these quantities result from the net motion of the sight line relative to the perturbing plasma. Amplitude changes in time or

in frequency are called *scintillation*, while all diffractive and refractive phenomena are the result of *scattering* of electromagnetic waves by electron density structures; scintillation and scattering are not synonyms. The temporal changes provide a sensitive probe of the smallest known structures in the intervening medium which have eluded physical description (*e.g.,* recent studies by **?** **?**, **?** **?**, **?**) since the beginning of pulsar research in 1968. The turbulent energy in these small scale structures in the interstellar medium may be a significant source of heat (*e.g.,* **?** **??**) as well as source of scattering of cosmic rays (*e.g.,* **?** **?**). One difficulty in the understanding of the small scale strutures in the interstellar medium is the uncertainty about the location of the structures along the line of sight and therefore an uncertainty in the mean properties of the perturbed plasma. In this paper we describe the recent variable propagation effects in the Crab pulsar and argue, as others have previously, that they result from plasma associated with nebula. In this case we have significant other information about the state of the material from optical observations which can aide theoretical analysis.

The propagation variations we will be discusssing have a historical precedence. In 1974-75 the dispersion measure, rotation measure and scattering of the Crab pulsar displayed extreme activity (**???**). The dispersion measure rose by 0.07 cm^{-3}pc and the Faraday rotation rose by 2 radians m^{-2} over several months. The scattering increased by an order of magnitude, and there was a deep, presumably refractive, amplitude null. These disturbances in the observed emission from the pulsar were ascribed to propagation through perturbed thermal plasma associated with the Crab nebula. **?**) had already argued on the basis of a two scattering screen model that the smaller variations of dispersion and Faraday rotation which they had observed were the result of nebular material. The variable screen was associated with the nebula, while the constant screen was associated with the general interstellar medium. **?**) compared VLBI observations of the apparent size to the scattering time scale and also showed the need for a scattering screen near the nebula. These authors suggested that the observed effects were the result of propagation through fine structure in the well-known filamentary material which was known to have structure on many length scales. More recently, precision observations of other pulsars have determined the level of dispersion measure variations in the general interstellar medium and found them to be significantly below that seen in the Crab (**???**).

In recent years there has been a second episode of large variations in the dispersion measure and scattering time scale (**?**). Column density variations of 0.1 cm^{-3} pc over time scales of months are seen. Starting farthest from the pulsar, potential sites for the perturbing plasma (and their radii from the pulsar) are: (a) the supernova blast wave forward and reverse shocks ($\sim$10 pc); (b) the shock and Rayleigh-Taylor unstable shell and shell fragments formed by the expanding synchrotron nebula (1-1.5 pc); (c) the synchrotron emitting particles (0-1 pc); and (d) the immediate environs of pulsar and relativistic pulsar wind shock (0.2 pc). Our estimate of the density of the synchrotron emitting electrons is 10^{-5} cm^{-3}, and so even the electrons in the weakly relativistic end of their energy distribution produce negligible dispersion in the hot interior of the nebula.

We will interpret our observations as the result of propagation through category (b) material, the unstable shell which forms filamentary structure, although admittedly this is in part because it is the structure about which we know the most from optical spectroscopy. Here we will distinguish between the diffuse high ionization material characterized by 'billowing' structures within a thick envelope region around the synchrotron nebula (**??**), and the low ionization, denser material which has a much smaller filling factor and is found over a range of radii. Both are loosely referred to as 'filaments' in the literature. **?**) argue that the high ionization material is the result of a shock between the synchrotron emitting internal gas and the external supernova ejecta and conclude that its radial cross section is $\sim 2 \times 10^{15}$ cm. Rayleigh-Taylor instabilities in the shock interface are the likely source of the cooler filaments (**??**). The typical density

of this material is 1000 cm^{-3} and the typical scale is $10^{16} - 10^{17}$ cm (**???**). Small structures or small variations within larger structures found in these optical studies could easily produce the changes in the 1974 and current episodes of large variability in propagation parameters. If the variations that we will discuss are the result of changes in the sight line column density through this filamentary material, then the transverse velocity of the pulsar-Earth sight line relative to the plasma is at least that of the pulsar, ∼135 km s^{-1} (**??**). The filament motions are radial (**?**) to within 100 km s^{-1}, and the shock velocity in the high ionization material is estimated to be ∼ 150 km s^{-1} (**?**). We will assume a value of 200 km s^{-1} for the characteristic transverse velocity of the sight line relative to the filaments for conversion from the time domain to the spatial domain. In this case, the estimated electron density of the observed perturbations is ∼ 1500 cm^{-3}, and their transverse length is $\sim 2 \times 10^{14}$ cm for single symmetric structures. This density is larger than, but comparable to, the estimates from optical line measurements. Smaller density variations on smaller length scales would be expected.

In 1997 October amidst the recent episode of large variations in dispersion measure and other plasma propagation parameters, a dispersion measure "jump" (a sudden change in less than one week) of 0.12 cm^{-3}pc was noticed in measurements with monitoring telescopes at both the NRAO[1] Green Bank and the University of Manchester Jodrell Bank sites (**??**). In fact, at the time of the jump pulses were simultaneously detected at both old and new DMs. Subsequently **?** noticed that prior to the dispersion event a faint "ghost" replica of the pulsed emission following the main pulse and interpulse components was seen for an interval of about two months. The phase of the ghost emission slowly converged toward that of the regular emission a few weeks before the dispersion jump. **?** discuss a geomtrical optics model for variable reflection of the signal from a plasma wall in the nebula, and infer a location of 2 pc from the pulsar. In this paper we interpret the observations with a full physical optics model of a plasma structure which has the rough form of an overdensity triangular prism.

While many of the observed phenomena can be explained by a plasma prism passing through the line of sight at the distance of the Crab nebula filaments, the occurrence of an unusual slowing down of the neutron star as well as the small but more conventional spinup glitch of the star two months later could provide an argument for consideration of plasma propagation in the vicinity of the star to allow for a causal connection. The fact that the ghost components of the main pulse and the interpulse are not always similar adds further confusion to the filament propagation interpretation. However, we argue in this paper that the propagation and spin disturbances are not causally connected.

In §2 we describe the Pulsar Monitoring Telescope facility at NRAO Green Bank along with our data collection and analysis procedures. In §3 we present a general description of the late 1997 events in the Crab data based on our observations at 327 MHz and 610 MHz. In a future work we will present a longer history of propagation parameters and their relation to the filamentary nebular material. This is followed in §4 by a discussion of the rotation history of the pulsar and in §5 by a presentation of our plasma prism model that explains most of the features of the event. In §6 we discuss the properties of the ghost emission along with our interpretation. In the concluding section we summarize our arguments for associating the observed phenomena with propagation effects in the Crab nebula's filamentary zone, and pose several questions that would motivate observations at the time of a future event.

---

[1]The National Radio Astronomy Observatory is a facility of the National Science Foundation operated under cooperative agreement by Associated Universities, Inc.

2. OBSERVATIONS WITH AN 85ft PULSAR MONITORING TELESCOPE

The observations described below were obtained with an 85ft (26m) diamter Pulsar Monitoring Telescope in Green Bank, WV. Pulsar observations were initiated on this telescope by Stinebring, Kaspi and their colleagues (e.g., **? ?**) in collaboration with the US Naval Observatory which supported the telescope operations at that time for geodetic work. Since then the Naval Research Laboratory contributed to operations, and currently a mixture of resources are applied to keep the system running. Room temperature receivers with linearly polarized feeds at 327 MHz and 610 MHz are mounted off axis and are then continuously available for use by offset pointing. The available bandwidths of the receivers are 10 MHz and 40 MHz, respectively, while our Crab observations used 8 MHz and 16 MHz, respectively. The Crab pulsar is observed twice per day at 610 MHz with 10-minute integrations (LST 06:05-06:50 & 10:35-11:20) and once per day at 327 MHz with 8.5-minute integrations (LST 06:55-07:35).

Average pulse profiles are obtained from each integration with the Green Bank-Berkeley Pulsar Processor (GBPP; *e.g.*, **? ?**). The GBPP coherently removes dispersion from pulsar radiation in real time by convolution in the time domain. Two othogonally polarized signals are each separated into 32 frequency channels which span the bandwidths defined above using analog and digital filter techniques. The dispersion removal restoring function for each channel has a maximum length of 1024 samples and the convolution processor, which employs a full-custom VLSI chip (**?**), uses low bit quantization. The multichannel data from this processor are dedispersed for the time delays between channels, linearized to remove the effects of quantization, normalized by the system temperature and summed over the two polarizations. Further reduction includes estimation of flux, pulse broadening, arrival times and other properties. Archival data from this monitoring program for the Crab and other pulsars are available upon request,[2] and please contact D. Backer if you are interested in use of the 85ft Pulsar Monitoring Telescope for new projects.

3. ANATOMY OF 327-MHz AND 610-MHz DATA

In Figure 1 we present a record of the pulse shape at 327 MHz during the interval of 1997 day 225 to day 365 (1997 Aug 12-Dec 31; MJD 50661-50813). The timing model that was used to align the daily average pulse profiles is given in Table 1. The morphology of the Crab's pulsed emission consists of three components: the precursor (P), main pulse (MP) and interpulse (IP) (**?**). The properties of these components – widths, relative amplitudes and relative locations – are typically obscured by the combined effects of interstellar scattering and instrumental impulse response. Our signal processor minimizes instrumental effects, and we have developed software to deconvolve the effects of interstellar scattering. Table 2 lists the intrinsic properties of the pulse components at our two observing frequencies. In Figure 1 the precursor, main pulse and interpulse components are overexposed to show a faint, "ghost", of the MP component that appears near phase 0.35 at 1997 day 240 and drifts toward phase 0.25 at day 275. A similar ghost of the IP component is evident with similar delays. We don't detect a ghost version of the precursor component, but it has a lower peak flux and where the MP is strongest, the location of the expected precursor ghost merges with the regular non-ghost emission. The dominant feature of Figure 1 is a jump in phase and change in signal character around day 300.

Figure 2 summarizes parameters of the 327-MHz profiles during the interval shown in Figure 1. We will refer to the signals before and after the jump as "old" (solid line) and "new" (dotted line), respectively.

[2]See also http://astro.berkeley.edu/~mpulsar

The old pulse peak amplitude begins steady, has a broad maximum around day 270 with two local maxima centered on day 265 and day 275, and then fades away by day 300 (Fig. 2a).

The new pulse amplitude rises steadily from day 290 to day 365. Estimates of the ghost component amplitude are difficult owing to its weakness and variable structure. The ratio of integrated flux, or pulse energy, of the ghost emission to the regular emission for the IP ranges from 2-6%. The relative arrival times of the old and new pulses are shown in Figure 2b. This indicates relative stability apart from the offset between old and new which is the result of the DM jump. Note the overlap of the old and the new pulse emission in Figure 2a,b. This will be interpreted in terms of *two* simultaneous propagation paths during the dispersion jump in §5. As the old pulse amplitude decreases during days 275-300 its position appears at later and later phases with a total shift between days 295 and 300 of 0.3 ms (Fig. 2b; also Fig. 5 which will be presented later). We discuss this shift in terms of an unusually large and rapid excursion of the intrinsic timing noise in the star in the following section after presentation of the 610-MHz data. The ghost component positions are shown in the second panel (open squares). These were estimated from the intensity peaks in Figure 1. Both old and new pulses show evidence of scattering with broadening by an exponential function whose time constant is given in Figure 2c. The new pulse is severely scattered in comparison with that of the old. Scattering by 0.3 ms is typical for this pulsar. There is little evidence for exponential broadening in the MP and IP ghost components.

In Figure 3 we present the corresponding record of the pulse shape at 610 MHz during the interval of 1997 day 225 to 1997 day 365. The timing model is the same as that used for Figure 1. The MP and IP are overexposed to show the faint precursor near phase 0.22 at 1997 day 225 and 0.3 at day 365. Intrinsic pulse morphology at 610 MHz is summarized in Table 2.

Figure 4a shows that the amplitudes of the old pulse components rose sharply starting on day 270. This rise was followed by local maxima on days 280 and 285 similar to what was reported above in the 327-MHz data, but shifted later in time. After day 290 the old amplitude subsides rapidly out to day 300 where detection is no longer possible. There is no evidence of any increase in the pulse broadening of this old emission as its amplitude subsides. The new emission appears diffusely around day 275, and we are able to fit for amplitudes and scattering times starting on day 315. The new emission amplitude rises steadily until day 355.

The old emission shows no evidence of scattering, and none would be expected if we scale the scattering detected at 327 MHz, typically 225 μs, to 610 MHz using a ν^{-4} law. The new emission is definitely scattered. From pulse deconvolutions we find exponential time constants ranging from 325 to 450 μs; Figure 4c plots a constant value of 340 μs. This scattering is much *larger* than that based on the 327-MHz results discussed above and using a ν^{-4} law. We return to this discrepancy in §5.3.

Starting on day 240 the "ghost" emission components at 610 MHz follow the MP and IP components and have a typical spread in rotational phase of 0.05. The leading edges of these components, which are their most clearly delineated feature, move steadily toward the main pulse and interpulse components (squares in Fig. 4b). Starting on day 260 the ghost emission components typically have the shape of an exponentially scattered pulse with time scale of approximately 1.2 ms. Figure 4 provides estimates of these exponential times along with the position and amplitude of the unscattered ghost emission. These parameters were obtained by first removing the strong, weakly scattered old emission in the MP and IP components, and then fitting for scattered MP and IP ghost components. Note that the total pulse energy in the ghost components is typically half of that in the regular components. This ratio is an order of magnitude larger than the ratio reported above for 327 MHz. They appear faint owing to the spreading of

the signal. On day 280 the ghost components bifurcate with a sharp subcomponent residing on the trailing edge of the regular MP and IP emission (*e.g.,* Fig. 10c which will be presented later) followed by a diffuse region of width 1 ms. We discuss the evolving location, relative amplitude and shape of ghost components in §6.

4. NEUTRON STAR ROTATION MODEL

Table 1 presents the rotation, astrometric and dispersion model parameters used to align signals for the images presented in Figures 1 and 3. These parameters lead to reasonably steady phases for the three months prior to the dispersion event in late 1997 October. We used template matching software for arrival time measurements that simultaneously fits for the decay time of an exponential broadening function which is the result of multipath propagation. Simultaneous solution for variable broadening is particularly important for the 327-MHz data. While this procedure is adequate for 327-MHz, **?**) show how at lower frequencies one must consider the effects of two scattering screens. The intrinsic profile that was used as our basic template was obtained during an epoch of low scattering. Our template matching software provided the amplitudes, positions and scattering times which are plotted in Figures 2 & 4. The arrival time parameters extracted from the data (Fig. 2b & 4b) were used to explore residual timing activity along with dispersion measure variations.

A simple extrapolation of the old pulse phases from days 215 to 290 to days 310 to 360 at the two frequencies (Fig. 2, 4) yields phase jumps in late 1997 October of 5.1 ms and 2.3 ms at 327 MHz and 610 MHz, respectively. If these jumps were solely the result of dispersion changes, then one could estimate the change from each frequency record independently. These estimates are 0.13 cm^{-3}pc and 0.21 cm^{-3}pc, respectively. We conclude that the changes in phase are not simply dispersive. Note that the effects of scattering have been removed in Figures 2b and 4b, and therefore we can't appeal to scattering as the source of the discrepancy. In fact, scattering would produce the opposite sense of discrepancy in the inferred dispersion measure jumps; *i.e.,* we would infer a larger DM jump for 327 MHz relative to 610 MHz. We conclude that there was an intrinsic slowing down[3] of the rotational phase of the pulsar around the time of the dispersion jump. This conclusion is in fact supported by independent measurements of the Crab pulsar at 1.4 GHz (**?**). The phase jumps given above yield a slow down of 1.2 ms along with a dispersion increase of 0.10 cm^{-3}pc. This leaves us with the unsatisfying coincidence of an unusual intrinsic timing event which is necessarily internal to the neutron star with a bizarre propagation event which is most naturally ascribed to plasma structures 1-2 pc distant from the pulsar.

The deceleration of the pulsar seems to have started around day 290 as we can just follow the old and lightly scattered pulse emission while the amplitude is extinguished during the onset of the dispersion event (Fig. 1,3). Fits to the interpulse position at both frequencies during this critical period are shown in Figure 5a. By focusing on just the data near the old interpulse position we were able to follow its location better than our general purpose template matching software. The 610-MHz arrival times have been adjusted by a constant 45 bins, or 1.2 ms, in this display. This shift is nominally the consequence of a dispersion measure difference from the assumed model (Table 1) of 0.14 cm^{-3}pc. Evident in Figure 5 is a frequency independent slow down of 0.22 ms during days 290-300 that we conclude is what begins to establish the new phase of the pulsar as the new emission appears at the new dispersion measure. Timing noise of the

[3]pulsar arrival times and model residuals are defined such that an increase in timing residual, or phase, relative to the model corresponds to a slowing down of the parent star.

Crab pulsar is characterized by a random walk in frequency with an amplitude that leads to 0.3 ms changes on time scales of a month; *e.g.,* see days 220-280 in Figure 5. The occurrence of an unusual spindown event – large amplitude in short time – at the very moment of the dispersion jump and amplitude null requires serious consideration about the possible coupling of these phenomena.

On MJD 50812 (1997 December 30) a "conventional" timing glitch occurred with $\delta\nu/\nu = 9 \times 10^{-9}$ (**?**). The decay timescale of the transient part of the glitch, 2.8 d, is also typical of past glitches. The beginning of this glitch is just detectable in the MP/IP on the last day of data presented in Figure 3.

In conclusion there are two timing events attributable to internal activity in the neutron star during this otherwise plasma propagation event. The probability of this "coincidence" is difficult to assess. Wong *et al.* report that the Crab has been involved in a cluster of rotation events during 1995-1999. This heightened "internal" activity coincides with the extended episode of large dispersion and scattering activity during which the particular events discussed in this paper have occurred. We proceed in this paper with the assumption that the coincidence of the two timing events with the dispersion/scattering events is the result of chance. While this assumption is plausible given the excess recent activities in both properties of the Crab emission, in a future analysis one might choose to explore a causal link between these seemingly disparate phenomena.

5. PLASMA PRISM MODEL

5.1. Basic model for DM changes

After removal of the neutron star rotation model which was presented in the previous section from the timing data, we fit the residuals for time variation of the dispersion measure (DM). The results are shown in Figure 6. The DM variations are characterized by a jump of $\delta\mathrm{DM}_\circ \simeq 0.12$ cm^{-3}pc that coincides with the interval around MJD 50700 when pulses are present at both dispersions as discussed in §3. Around the time of the jump the results presented in Figure 5 provide more accuracy owing to the careful fitting of individual pulse components. After the jump the DM steadily declines with most of the jump amplitude lost over $T \sim 250$ days. There are small increases centered on MJDs 50825 and 50890 (Fig. 6). A slower decline has continued to MJD 51300. We interpret the sudden rise and steady decline as evidence for the passage of a uniform density triangular prism of plasma through our sight line to the pulsar. One lateral face of the prism must be parallel to the line of sight to provide the observed jump when the geometric sight line enters the prism owing to relative motions of pulsar, prism and observer (see inset in Fig. 7). The physical nature of the prism will be addressed briefly in our conclusion. Here we are concerned with the radio wave propagation through the prism as it crosses our sight line to the pulsar.

The steady DM gradient during the 250-day interval after the DM jump can be converted into a frequency dependent refraction angle $\theta_r(\nu)$ in the prism. The triangular plasma prism model has three important parameters: the extent transverse to the sight line L which we equate to the product of the motion of the sight line transverse to the pulsar direction $V_\perp$ and T; the extent along the sight line at the "thick" end of the prism fL, and an excess electron density $\delta n_e \equiv \delta\mathrm{DM}_\circ / fL$. The two length measurements are the height and the base of the assumed isosceles triangular cross section of the prism. The effect of this prism on propagation can be accurately calculated based on the equivalent phase screen $\Phi(x, y)$ that is derived by line of sight integration of the electrical phase through the dispersive prism:

$$\Phi(t) \equiv \lambda r_e \, \delta\mathrm{DM(t)}, \tag{1}$$

which leads to the refraction angle

$$\theta_r = k^{-1}\nabla\Phi \tag{2a}$$

$$\theta_r = \frac{\lambda^2 r_e\ \delta\mathrm{DM}_\circ}{2\pi V_\perp T}. \tag{2b}$$

Quantitatively the refraction angle through the prism at 327 MHz is

$$\theta_r(327\ \mathrm{MHz}) = 0.35\ \mu\mathrm{rad}\ V_{\perp,100}^{-1}, \tag{3}$$

where the perpendicular velocity is expressed in units of 100 km s^{-1}. The phase velocity in cold plasma exceeds c and therefore the sign of the refraction is such that an *overlap* in time is expected for the direct and refracted signals, which is what we reported in the previous section. We return to this point in the following section that presents a simulation of the optics.

The geometric time delay, δt_r, resulting from this refraction is very likely small in comparison with the several-ms dispersion delay (Fig. 5):

$$\delta t_r^{327} = z(1-z)D\theta_r^2/c = 20\ \mu\mathrm{s}\ z_{0.001}V_{\perp,100}^{-2}, \tag{4}$$

where the location of the prism as a fraction of the distance between the pulsar and the Earth z is expressed in units of 0.001 (2 pc), appropriate for the filamentary interface around the Crab synchrotron nebula. The frequency dependence of this refractive delay is nominally ν^{-4}, and therefore in future events it could be separated from a dispersion delay with sufficient frequency sampling.

Refraction in the prism will lead to a signal path that depends on radio frequency. The transverse displacement of the image path at the location of the perturbing plasma is $zD\theta_r \sim 2\times10^{12}$ cm $z_{0.001}V_{\perp,100}^{-1}$ at 327 MHz. This displacement toward the thin end of the prism results in a smaller dispersion measure for 327 MHz relative to that for 610 MHz at any instant. An estimate of the size of this effect using this displacement and the observed gradient is 0.0011 cm^{-3}pc $z_{0.001}V_{\perp,100}^{-2}$ which also contributes a small time delay of 40 μs $V_{\perp,100}^{-2}z_{0.001}$. This effect will not contribute significantly to the non-dispersive time delays estimated from the extrapolated rotation model of the neutron star presented in the previous section if the site of the dispersion changes is in the filament zone of the nebula.

For an aspect ratio $f = 1$ and $V_\perp = 100$ km s^{-1} the excess electron density in the prism is 1700 cm^{-3}, and the emission measure for this choice of parameters is small, $\sim$2 cm^{-6} pc, relative to that of the filaments. If the prism extent along the sight line is several times that in the transverse direction ($f \sim 3$) and if the transverse velocity is as large as 300 km s^{-1}, then the prism density can be as low as 170 cm^{-3}. As the densities of the ionized filaments which have scale size of 10^{16-17} cm are estimated to be around 1000 cm^{-3}, a much smaller density perturbation on the much smaller scale of the prism is likely, and possible, given this discussion of geometry and motion. Thus a factor of ~ 3 is favored.

5.2. Transverse velocity from refractive amplitude variations

The variable amplitude of the pulsed emission can be used to constrain the transverse motion of the plasma prism if we attribute these changes to refractive focusing and defocusing. **?**) provide a useful description of the refractive optics of a Gaussian plasma lens. The refractive gain is assumed to be single valued (near field) and is a function of the second derivative of the phase accumulated after propagation through the lens. The amplitude drops into a deep null over about 10 days (290 to 300) at 327 MHz and

over a shorter interval at 610 MHz (Fig. 2c,4c). We attribute this to the spreading of rays by the defocusing power of the phase screen just ahead of the plasma prism. Following **?**) the gain which results from a refractive 1D parabolic phase variation located at zD along the sight line from the pulsar is

$$G_x = [1 - z(1-z)Dk^{-1}\nabla^2\Phi]^{-1}. \quad (5)$$

With $\nabla^2\Phi$ estimated from $\delta\mathrm{DM}_\circ/(V_\perp\ \delta T)^2$ and a gain of 0.1-0.2 and $\delta T = 10$ d, we estimate that the transverse velocity is

$$\hat{V}_\perp = 150 \text{ km s}^{-1}\ \sqrt{z_{0.001}}. \quad (6)$$

The shorter time scale for the decrease at 610 MHz is consistent with expectations of this simple model. Furthermore, there is evidence for a parabolic term in the phase owing to the observed variations of dispersion measure in Figures 5 & 6 along with its conversion to phase (eq. 1). For our model prism the dominant parabolic phase variation is most likely directed normal to the projected edge of the prism and not along the direction of the motion of the sight line; see Figure 7. The velocity estimated from this calculation is then a lower limit to the true transverse motion of the prism.

What is the transverse motion of the sight line to the pulsar relative to the possible filamentary material in front of it? If the material is just radially expanding, then there would be one contribution to the transverse motion from the pulsar motion, 135 km s^{-1} (**??**). This will be reduced by a component of the radial motion of the filaments which results from the misalignment of the current pulsar location from the expansion center. For the estimated 10″ misalignment (**?**) this amounts to 100 km s^{-1} for material at 1.5 pc moving at 1500 km s^{-1}. The net motion is then only 35 km s^{-1}. There will be an additional contribution from the random velocity of the filaments causing the propagation effects discussed in this paper, assuming that they are indeed the site of the perturbations. **?**) makes a strong case that the non-radial motions of the isolated filaments which she studied are less than 300 km s^{-1} and are typically 70 km s^{-1}. Her reasoning is that a well defined convergent point of expansion would not be found if non-radial motions were larger. The further conclusion from her study is that the expansion velocities range from about 500 km s^{-1} up to 1500 km s^{-1} which corresponds to radii from 0.5 pc to 1.5 pc, respectively. The filaments nearest the pulsar in Trimble's study – numbered 158, 160, 208 and 209 – have observed transverse motions of 47 to 267 km s^{-1}.

More recent studies of the Crab nebula filamentary material have come to the conclusion that many features can be attributed to Rayleigh-Taylor MHD instabilities (**???**). The low-density, synchrotron emitting matter driven by the pulsar is pressing on the denser supernova ejecta. Fingers or sheets of ejecta matter drip into the interior along quasi-radial paths. These authors estimate velocites of the shock interface of 150 km s^{-1}. The Alfvèn velocity is significantly smaller, v_A =20 km s$^{-1}B_{-3.5}\sqrt{Zn_3}$, where the magnetic field $B_{-4.5}$ is in units of 3×10^{-4} G, the density n_3 is in units of 10^3 cm^{-3} and the atomic number Z may be as large as 4 if the relevant filament is dominated by Helium (**?**). Both the shock velocity and a component of the velocity from any non-radial motion of the unstable interface could contribute to the transverse velocity that we need to convert our temporal record to a spatial record. A second epoch of HST imaging is planned that will allow much higher resolution study of motions of the small scale filamentary features (Hester, 1999 personal communication).

On a larger scale most of the filamentary material which would be along our sight line to the pulsar has been associated with a constricted toroidal region around the synchrotron nebula that is associated with the 'dark bays' in the synchrotron emission (**??**). These authors suggest the possibility that this is the result of a circumstellar disk that predated the Crab SN. While larger transverse velocities might be associated with this morphology, Trimble's observational limits on motions of specific filamentary features remains. In summary, we choose to use 200 km s^{-1} for our length to time conversions.

The amplitude of the 'old' signal has a broad maximum that extends over 40 (20) days centered on day 270 (285) at 327 (610) MHz, respectively (see Fig. 2c,4c). There is some evidence for two local maxima with dips at day 270 (281) and preceding and following higher values. This peaking, and possibly double peaking, of the amplitude has the appearance of a caustic crossing event that can be associated with the subsequent sharp loss of amplitude around the time of the dispersion jump which was discussed earlier in our estimate of the transverse velocity. **?**) analyze the optics of a Gaussian plasma lens and show how it can reproduce the amplitude signature of extreme scattering events. The equivalent lens at the time of the jump which strongly defocuses the radiation will lead to a pileup of amplitude prior to the jump. The absence of a similar caustic crossing event on the egress can be attributed to asymmetries of the equivalent phase screen in the two transverse dimensions.

5.3. Broadening from multipath propagation

The new pulse viewed through the prism is broadened at 327 MHz by an exponential function with a typical time constant of $\tau_s = 2.1$ ms (§3; Fig. 2c). If we equate this broadening to the simple thin screen result

$$\tau_s = z(1-z)D\theta_s^2/c \tag{7}$$

with $\theta_s = \lambda/l_\circ$ as the scattering angle of the screen, then the coherence length scale of the screen is $l_\circ = 3 \times 10^3$ cm for 327 MHz and $z = 0.001$. At $z = 0.001$ the scale of the first Fresnel zone is $a_{\rm F} = 2 \times 10^{10}$ cm, and, owing to the inequality $l_\circ << a_{\rm F}$, we expect strong diffraction effects. The same condition holds at 610 MHz. Phase fluctuations on this small scale can result from either a turbulence spectrum extending down to this scale or from gradients of structures on larger scales.

The scaling of the new pulse broadening can indicate the slope of the 'turbulence' (average density fluctuation) spectrum **?**). Using the results from Figures 2c & 4c we find an electron density power law slope of -6, much steeper than the Kolmogorov slope of 11/3 and steeper than the slope expected if we are sampling beyond the wavenumber cutoff or inner scale which is -4. An alternative interpretation is that the sight lines are sampling different material (Fig. 7). However the ratio of pulse broadening at the two frequencies does not change significantly during 1997 November and December. If there were significant variations transverse to the path of line of sight through the prism, one would expect comparable variations along the line of sight. A further alternative is the idea raised by Cordes (1998, personal communication) that the fluctuations are intermittent, and therefore the full extent of broadening is not equally attained at the two frequencies. The signature of this effect would be a shallower dependence of pulse broadening on frequency than -4. But this model would also predict truncated exponential pulse broadening functions and large variability which are not observed. In future observations during a similar episode of enhanced scattering multi-wavelength studies are essential to establish the frequency dependence of pulse broadening.

?) show that at high angular resolution many filaments appear to be smooth Rayleigh-Taylor fingers which are falling into the synchrotron nebula. In their model these fingers are stabilized by a transverse magnetic field in the interface against breakup into smaller scales by Kelvin-Helmholtz instability. On the other hand, they also show some filaments with fine structure indicative of Kelvin-Helmholtz instabilities. The steep fluctuation spectrum in the prism inferred above from pulse broadening would favor the presence of Kelvin-Helmholtz instabilities continuing to small scales. **?**) provide an important high spatial resolution simulation of the growth of these MHD instabilities for various geometries and magnetic field strengths. In the future we plan to compare the small scale column density, scattering and Faraday rotation changes of the Crab pulsar with results obtained from these computer simulations.

6. MODEL FOR THE GHOST EMISSION COMPONENTS

The ghost emission components described in §3 have arrival times that are mainly achromatic. This property of the ghost emission can be explained if the arrival time is dominated by geometric path delay. The plasma prism model described in §5 will lead to multiple imaging, and therefore to multiple pulses if the resultant geometric relative delays are large with respect to the pulse component width. As an aside, if the relative delays were less than the width, interference would be observed similar to that reported by **?**) and **?**), and multiple structure might be detected in the narrow giant pulses (**?**). We have already described how refraction in a simple plasma prism can explain the presence of simultaneous emission at new and old dispersion measures simultaneously. Here we describe how the ghost emission is consistent with it being the result of a third image which should be present following the 'odd number of images' optics rule that has been frequently applied to gravitational lensing. The ghost emission components also show evidence for multipath broadening at 610 MHz, and yet are not strongly scattered at 327 MHz. The model discussed below proposes a possible solution to this discrepancy.

Our explanation for the ghost emission requires further analysis of the phase screen that results from the plasma prism model introduced in §5. The dispersion record and the amplitude modulation indicated the presence of linear and quadratic properties of the screen both ahead of and in the prism. The full phase screen required for analysis of wave propagation includes effects of both propagation through the plasma and the geometric path length. The geometric path length contributes a parabolic "Fresnel bowl" of phase centered on the sight line:

$$\Phi_{\rm F}(x,y) = A[(x - V_\perp t)^2 + y^2], \tag{8}$$

where $A \equiv \pi/z(1-z)\lambda D$ establishes the scale of the quadratic Fresnel phase bowl in radians by dividing by the square of the radius of the first Fresnel zone. We place the leading (thick) edge of plasma prism at $(x = b, y = 0)$ with an orientation angle in the xy-plane of ζ with respect to the x-axis. The equation for the prism leading edge is then $y_p = \tan\zeta \cdot (x - b)$. We give the prism leading edge a sinusoidal density profile which leads to sinusoidal phase profile:

$$\Phi_{\rm P} = \frac{B}{2}\left(1 - \sin[\pi\frac{(x-b)}{w}\cos\zeta + \pi(\frac{y}{w})\sin\zeta]\right), \tag{9}$$

where the half width of the prism's leading edge w is $V_\perp\ \delta T$ which defines the edge width δT, and $B \equiv \lambda r_e\ \delta{\rm DM}_\circ$ sets the phase scale of the prism (see eq. 1). A cross cut of the total phase relative to the geometric line of sight at $x - V_\perp t$ is shown in Figure 8. If we set $y = \zeta = 0$, then

$$\nabla\Phi = 2a(x - V_\perp t) - \frac{\pi b}{2w}\cos\left[\pi(\frac{x-b}{w})\right] = 0 \tag{10}$$

establishes points of stationary phase as a function of frequency. These stationary phase points can then be used to calculate the corresponding geometric delays as a function of frequency and time. The roots of $x - V_\perp t$ on either side of b which give the locations of stationary phases $(x - V_\perp t)_s$ are labeled with II,III in Figure 8. Signals from point II pass through the leading edge of the prism, and therefore have a dispersive delay similar to that of the old emission; point III signals pass through the prism and have the extra dispersion of the prism. Nominally these points are close to $x - V_\perp t = b$ where the geometric delay is

$$t_{\rm ghost,geo} = z(1-z)(x - V_\perp t)_s^2/cD. \tag{11}$$

Association of image II with the ghost emission explains the quadratic and nearly achromatic properties of what has been observed.

This model of the optics was used to simulate a sequence of pulse arrival times. The dispersion record was used to estimate Φ_P with the following elements: a constant; followed by a cosinusoidal decrease over 60 days preceding the jump with an amplitude of 0.01 $cm^{-3}pc$; followed by a cosinusoidal increase over 15 days with an amplitude of 0.1 $cm^{-3}pc$; and a final linear decay over 250 days. This phase screen was added to the quadratic Fresnel term with the screen placed at $z = 0.001$. The stationary phase points were then located for each day using a transverse velocity of 200 km s^{-1}. At each stationary phase point dispersive delays at the two frequencies and the geometric delay were tabulated. Figure 9 displays the relative arrival times of the observed pulses at the two frequencies as a function of time using the enumeration of stationary phase points in Figure 8. The simulation, which was obtained with very little iteration of the model parameters, is reasonably consistent with the observations in Figures 1-4. Note that the 327-MHz ghost emission arrives slightly earlier than that at 610 MHz owing in part to the decrease in dispersion measure prior to the moment when the geometric sight line enters the prism.

The absence of the pulse broadening effects of scattering (diffraction) in the 327-MHz ghost emission is curious given the scattering which is evident in the 610-MHz ghost emission (Fig. 4c). The plasma prism model analyzed here only includes linear and quadratic phase terms. The prism itself is very turbulent as shown by the pulse broadening of the new signal (Fig. 2c,4c). The stationary phase points for the ghost at 327 MHz (II) will pass through less of the prism than at 610 MHz which can contribute to the absence. Furthermore it may be difficult to detect parts of the signal that are very heavily scattered at 327 MHz. The very weak amplitude of the 327-MHz ghost emission relative to 610 MHz (§3) suggests that we are observing along a low gain path which has the correct refraction angle for us to observe and has negligible diffractive scattering.

Figure 10 provides three examples of 610-MHz ghost components. The regular MP and IP emission has been subtracted using a template of the pulse derived from earlier observations (Table 2) along with the exponential broadening from scattering as determined at 327 MHz (Fig. 2c). The scales are set such that the "old" MP component peak amplitude is 1.0. Subtraction of the old emission is not always perfect at the level of 5%. Owing to the narrow width of the MP and IP, we are confident that the imperfect subtraction has no effect on the ghost emission profile in these data. The result for day 270 demonstrates a typical result: the ghost of the MP is identical in shape, relative position and relative amplitude to that of the IP. This provides strong support for the conclusion that the ghost emission is a replica of the entire pulse delayed by extra path length along which the scattering properties are significantly different to that of the direct path.

However there are days when the MP and IP ghost emissions are dissimilar. On day 262, the ratio of the IP ghost emission to that of the main pulse is much less than expected from the delayed and scattered replica hypothesis. On day 293 the shapes of the MP and IP ghost emission are dissimilar – the IP extends longer than the MP. The shape of either of the ghost components is not simply an exponentially broadened version of the undelayed counterpart. Within the context of our plasma prism model non-exponential scattering profiles are simple to explain. For example, Cordes (1998, personal communication) has explored the effects of small-scale intermittency on scattered pulses. By small scale he means that the turbulent plasma does not fill the diffractive scale, $l_d = z\theta_s$. If so, one or more highly truncated exponential pulses would be observed from individual "screenlets" with their associated geometric delays and scattering time constants. This incomplete scattering situation was also discussed by **?**) to explain the odd pulse shapes observed during the earlier episode of extreme scattering.

The occasionally dissimilar shape of the MP and IP ghost components may indicate that the phase screen is effectively resolving their angular separation. MP and IP emission is most likely from the outer

magnetosphere. **?**) and **?**) provide recent models of the high frequency emission, and one generally assumes that the sites of the MP and IP radio emission are coincident with the sites of the corresponding high frequency components. In the **?** model the MP and IP will have a projected separation at the plane of the neutron star center which is comparable to that of the light cylinder radius, 1500 km. At the distance of our hypothesized phase screen, 1-1.5 pc, this corresponds to 7 μas. In the **?** polar cap model no such offset is expected. In §5 we estimated that the average refraction angle in the plasma prism is of order 0.35 μas at 327 MHz (eq. 3) which is then ~ 0.1 μas at 610 MHz. The presence of significantly larger gradients in smaller regions might be possible. If so, these could lead to significantly different refractive gains for the ghost MP and IP emission. Note that while the separation between paths from the MP and IP may be much larger than $l_\circ \sim 10^{3-4}$ cm, the size of the diffractive disk $z\theta_s(1-z)D \sim 10^{11-12}$ cm is much larger than the likely path separation. Therefore there is little change expected in the diffraction of the two pulse components. The perturbed optics of the filamentary zone of the nebula during this epoch may thus be resolving the magnetospheric emission sites and therefore supporting high altitude emission models.

7. CONCLUSIONS

In this paper we have:

(1) reported on an anomalous events in the record of the Crab pulsar during the second half of 1997 which involve rapid changes in the pulsar's flux, dispersion measure and pulse broadening time as well as the appearance of ghost emission;

(2) found what appears to be a slowing down of the rotational phase of the parent neutron star at the time of the propagation event which we tentatively conclude is coincidental owing to the current clustering of rotation events;

(3) modeled the flux, dispersion measure and pulse broadening time changes and the ghost emission as the refractive and diffractive effects of a plasma prism which crossed the sight line and is located in the filamentary zone of the Crab nebula; and

(4) concluded that the corrupted optics of the plasma prism has provided sufficient resolution to distinguish the apparent locations of the main pulse and interpulse which lends support to outer magnetosphere models.

These results provide important constraints on the small scale density structures for detailed simulations of the three dimensional plasma dynamics in the filamentary zone of the Crab nebula. The results complement high resolution studies of line emission which can provide three dimensional motions and physical conditions of the same material at reduced spatial resolution.

During the next episode of strongly perturbed propagation a number of supporting observations are needed. High angular resolution measurements with VLBI at wavelengths down to 1m and longer will provide limits on, or measurements of, both the separation of the direct and ghost emission and the apparent angular diameter which will improve the inferences about the screen's location and its transverse motion. Accurately calibrated polarimetry will provide measures of Faraday rotation which samples the radial component of the magnetic field. The nominal overpressure in the plasma prism could be balanced by magnetic pressure surrounding it which could lead in turn to a distinct Faraday rotation signature. Alternatively the prism may be part of a evolving shock structure. Our current polarimetry data will be studied for evidence of variable Faraday rotation, but the offset feed configuration is known to have poor polarization properties. Sampling pulse shape and arrival time over more radio frequencies will allow better

assessment of dispersive, refractive and diffractive effects.

We are grateful to the NRAO staff for maintenance of the 85ft Pulsar Monitoring Telescope and for assistance with our observational program. This monitoring effort has also been supported through the Naval Research Laboratory and US Naval Observatory activities with the Green Bank 85ft telescopes. We thank Graham Smith and Andrew Lyne for sharing the results of their preliminary investigations of the Crab events using their and our data, and look forward to further synthesis of all measurements. Our effort has been supported from NSF grants AST-9307913 in the past and currently AST-9820662.

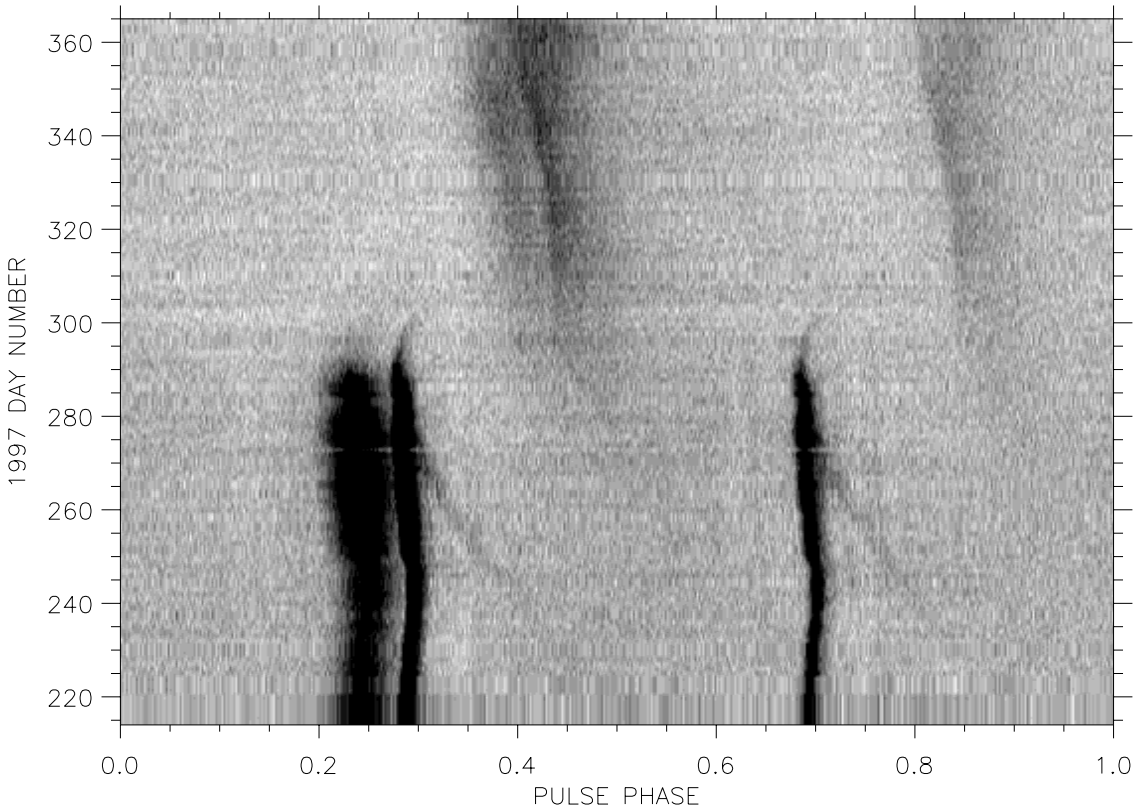

Fig. 1.— Image of pulsar flux at 327 MHz obtained with an 85ft telescope at NRAO Green Bank. The dispersion jump reported in this paper occurs around day 295, and a rotation glitch has just started on day 365.

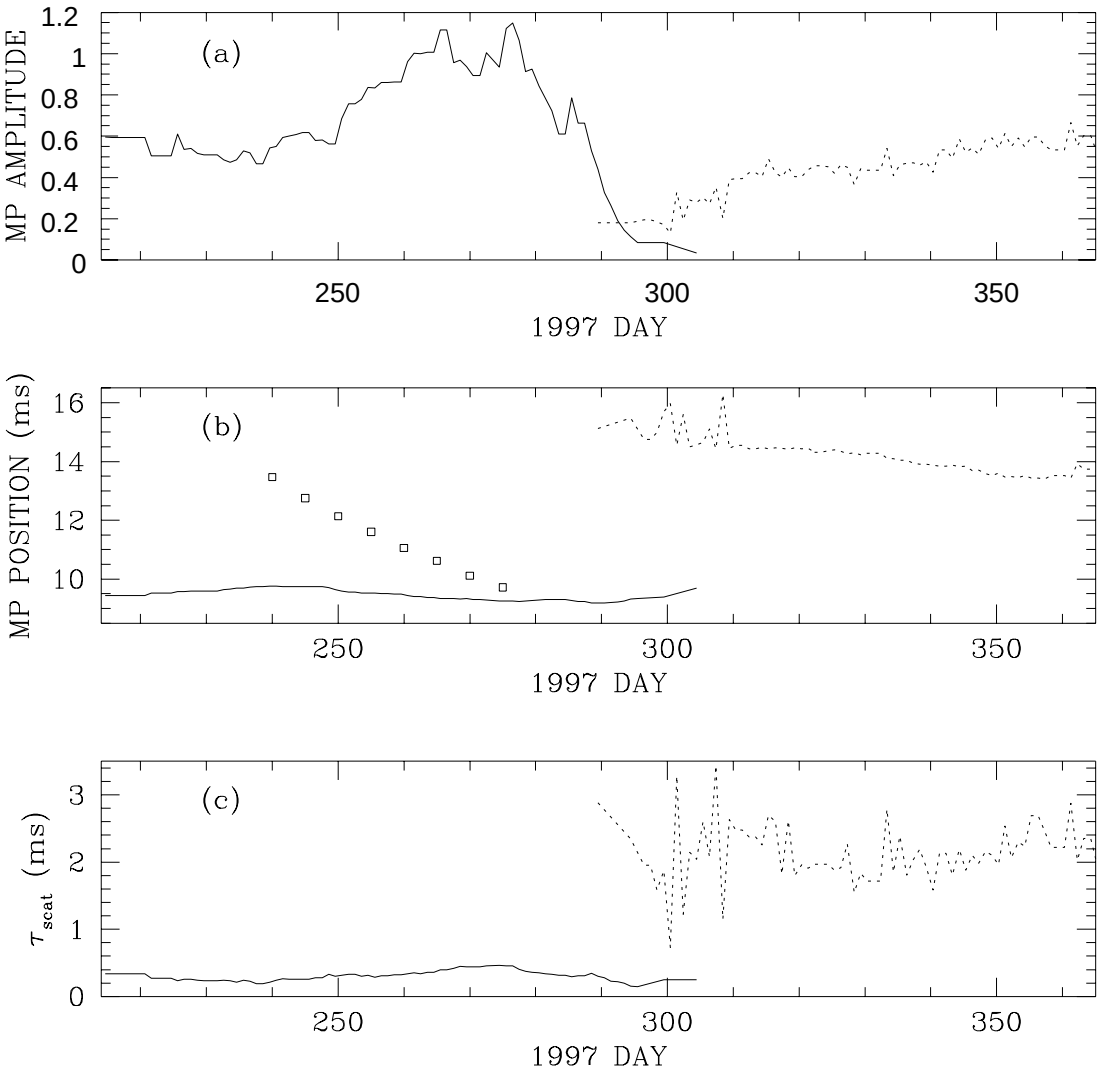

Fig. 2.— Observational parameters of the 327-MHz data. The solid and dotted lines present parameters of the "old" and "new" pulses, respectively: (a) amplitude of main pulse; (b) position of main pulse; and (c) exponential pulse broadening time scale. In (b) the locations of the strongest "ghost" component emission are shown with squares.

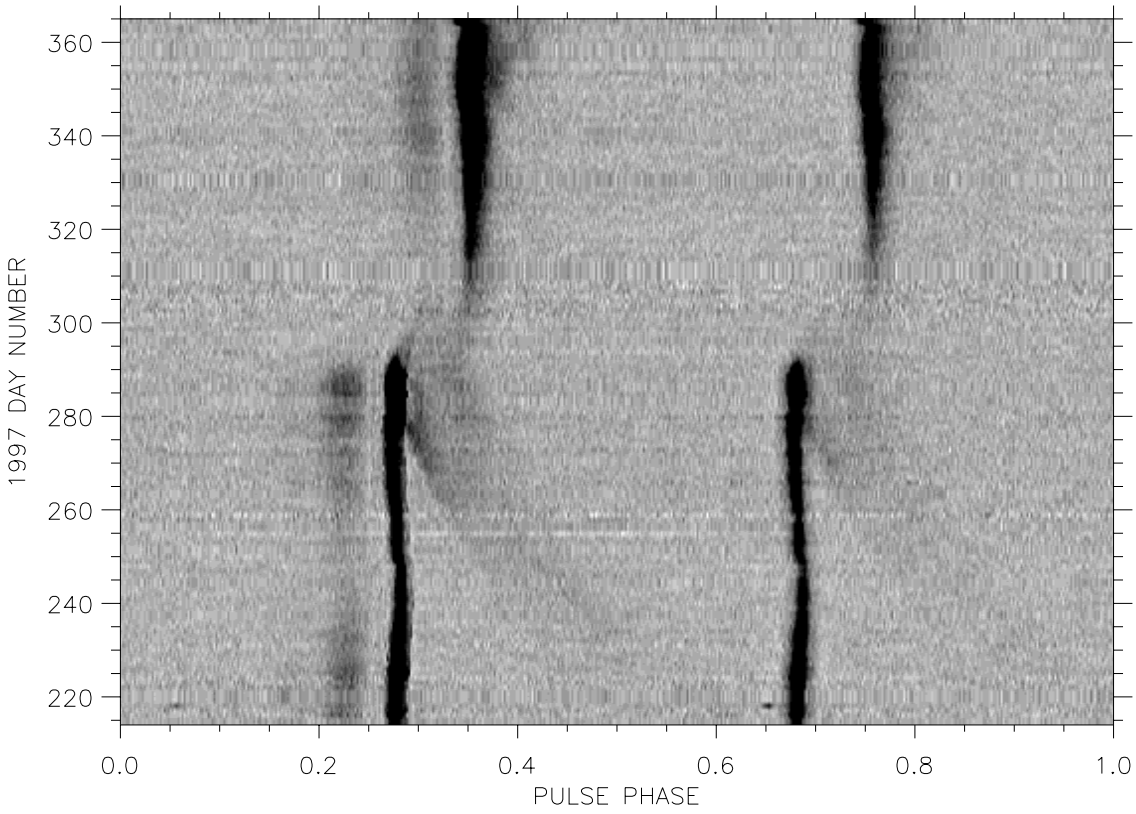

Fig. 3.— Image of pulsar flux at 610 MHz obtained with an 85ft telescope at NRAO Green Bank. The dispersion jump occurs around day 295, and a rotation glitch has just started on day 365.

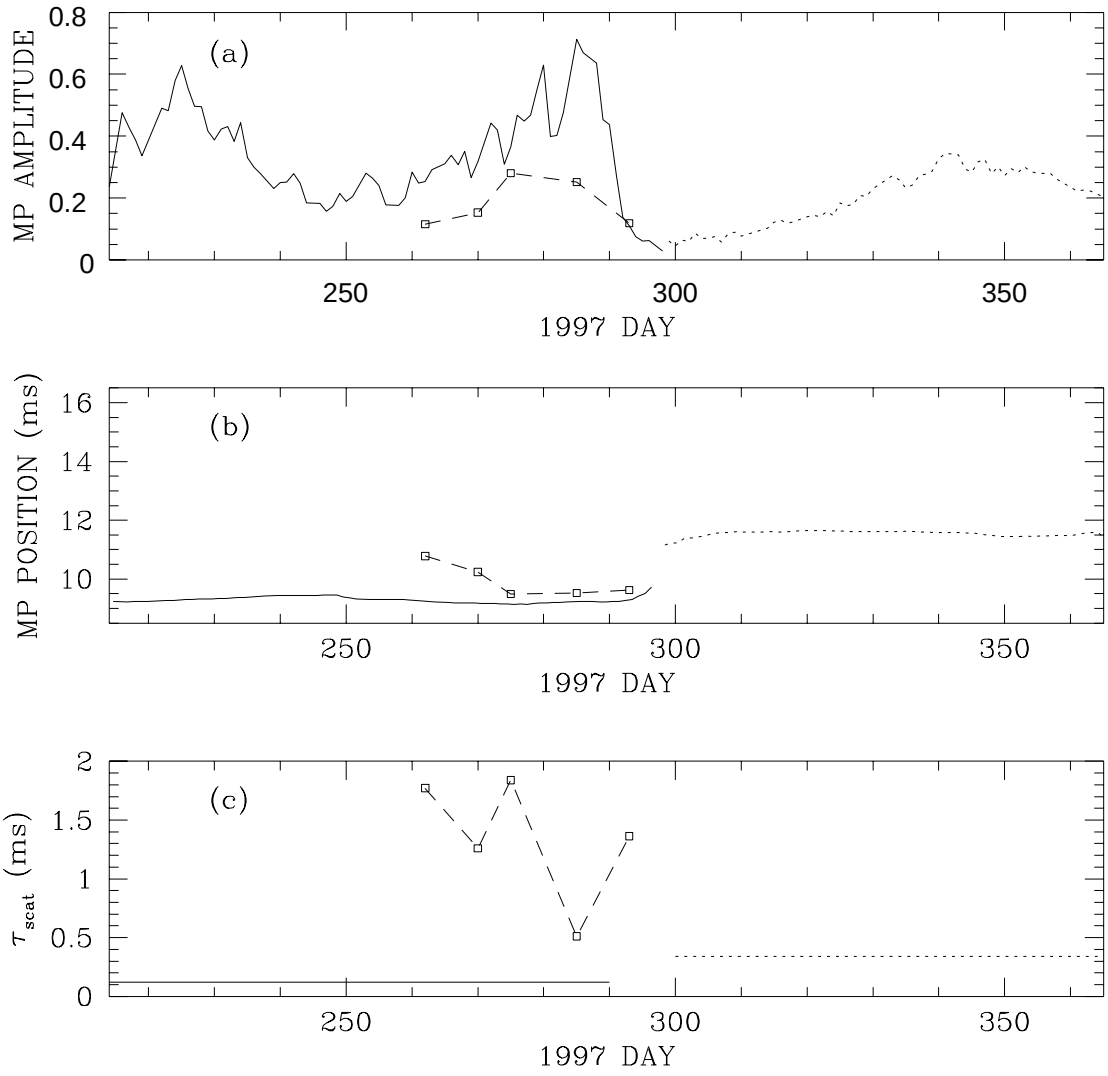

Fig. 4.— Observational parameters of the 610-MHz event. The solid, dashed and dotted lines present parameters of the "old", "ghost" and "new" interpulse components, respectively: (a) amplitude of main pulse; (b) position of main pulse; and (c) exponential pulse broadening time scale.

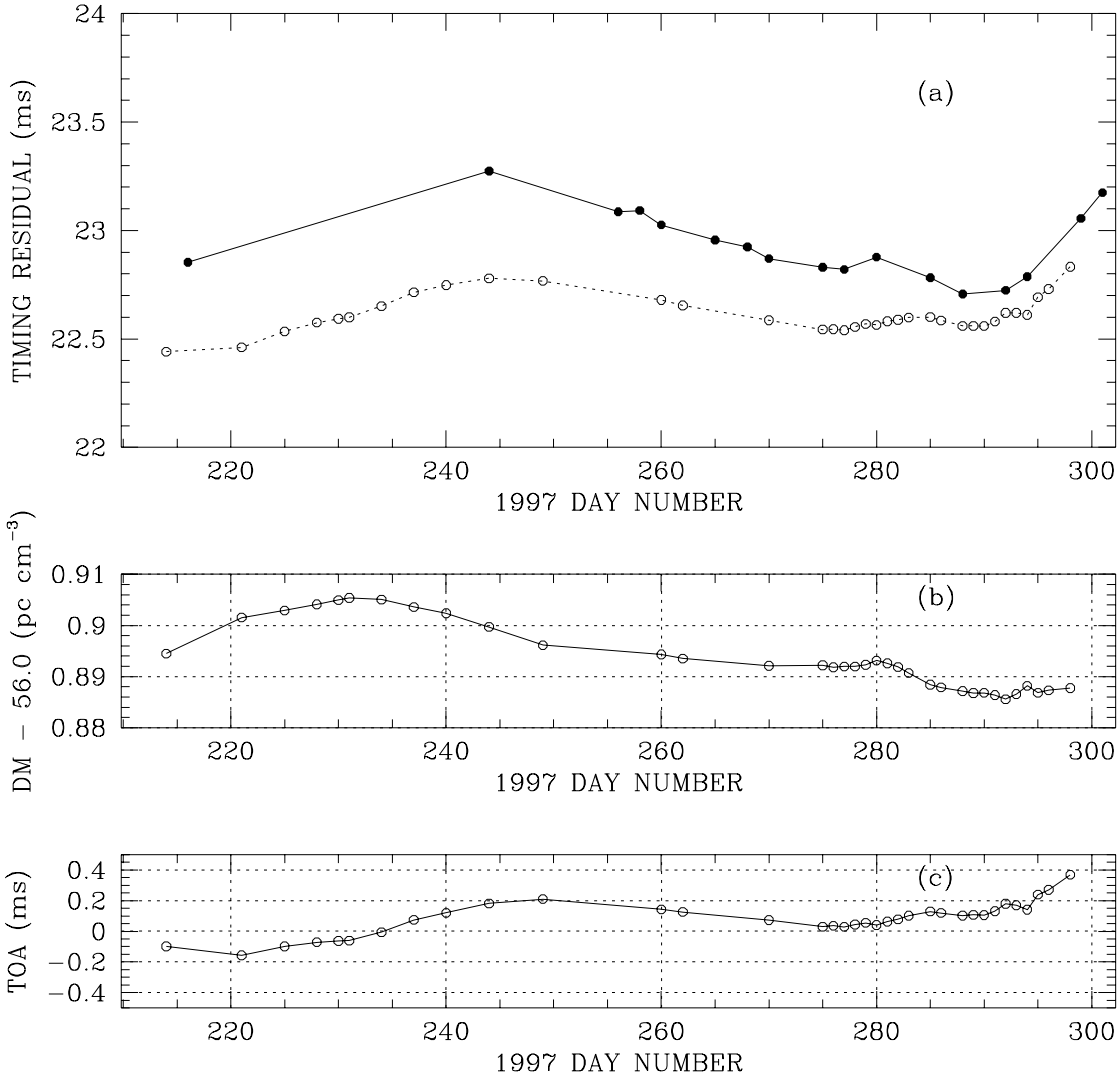

Fig. 5.— In (a) the arrival times at 327 MHz and 610 MHz from Figures 1-4 are compared; the 610 MHz times have been shifted by 1 ms which corresponds to a small shift in the dispersion relative to that in Table 1. The times are then decomposed into residual dispersion measure in (b) and infinite frequency timing residual in (c).

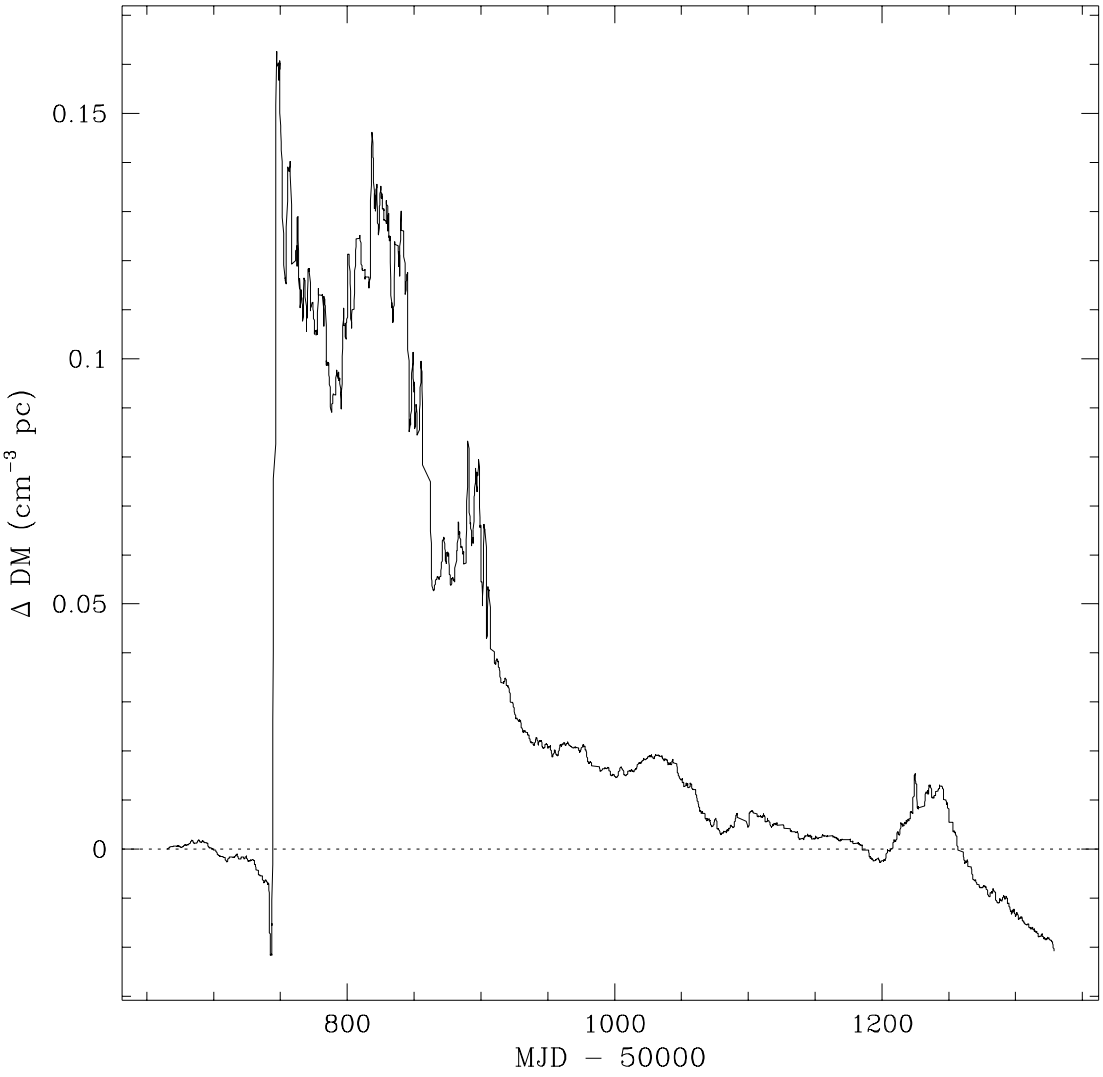

Fig. 6.— Dispersion measure variations from NRAO Green Bank observations at 327 MHz and 610 MHz. The influence of scattering has been removed. The data have been smoothed with 7-d running average. The dispersion jump occurred during MJD 50736-750 (1997 October 15-29; days 288-302). Dispersion measurements at times closest to the jump are difficult owing to the low flux and extreme values of exponential pulse broadening (scattering) at 327 MHz.

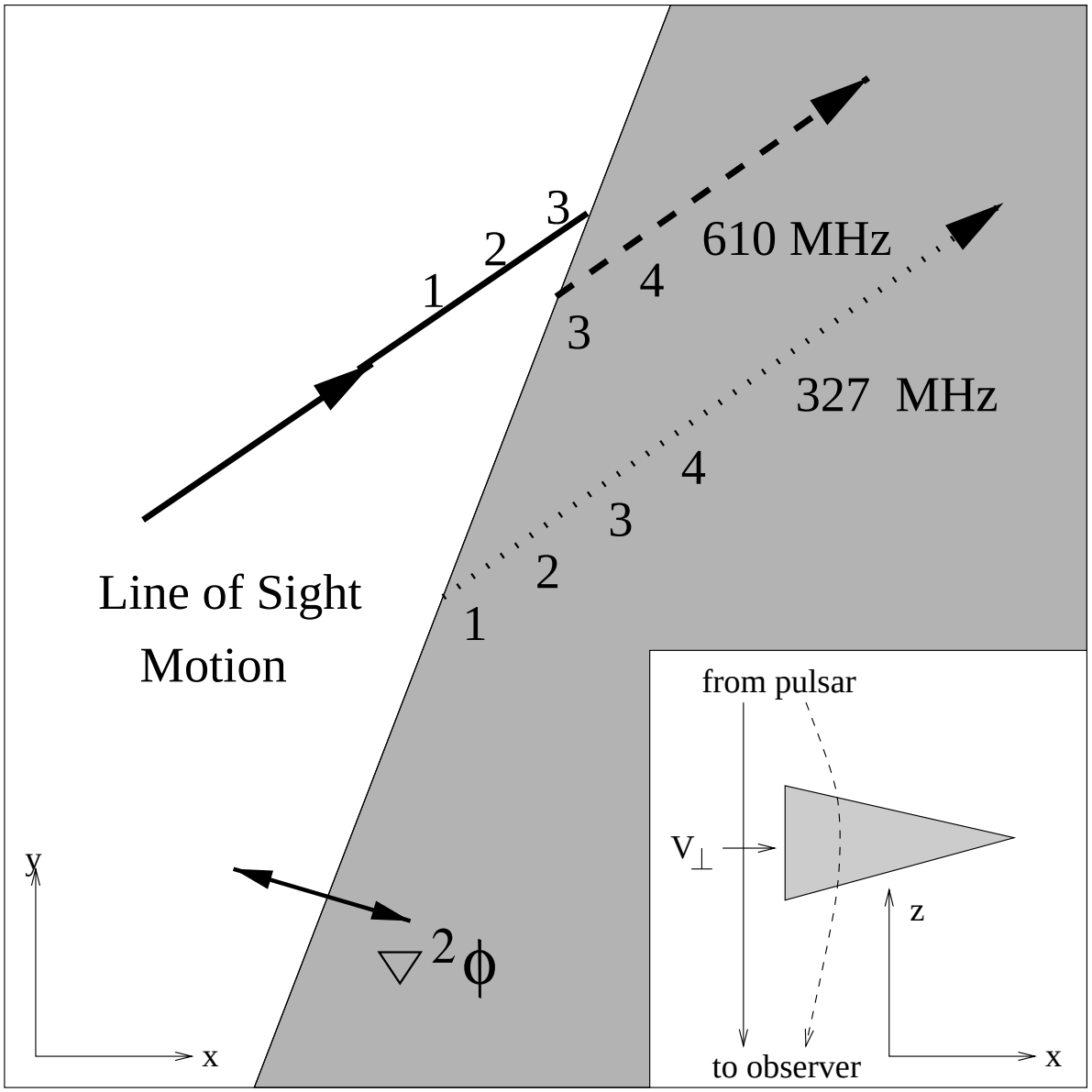

Fig. 7.— Model of motion of sight line and refracted sight lines at two frequencies across the sky (xy plane) relative to a plasma prism (shaded). The numbers indicate sequential locations of the direct and refracted sight lines as they approach and traverse the prism, respectively. The inset diagram (xz plane) shows the direct sight line and a sight line refracted through the triangular prism. The expected direction of the maximum second derivative of the phase screen is shown perpendicular to edge of prism.

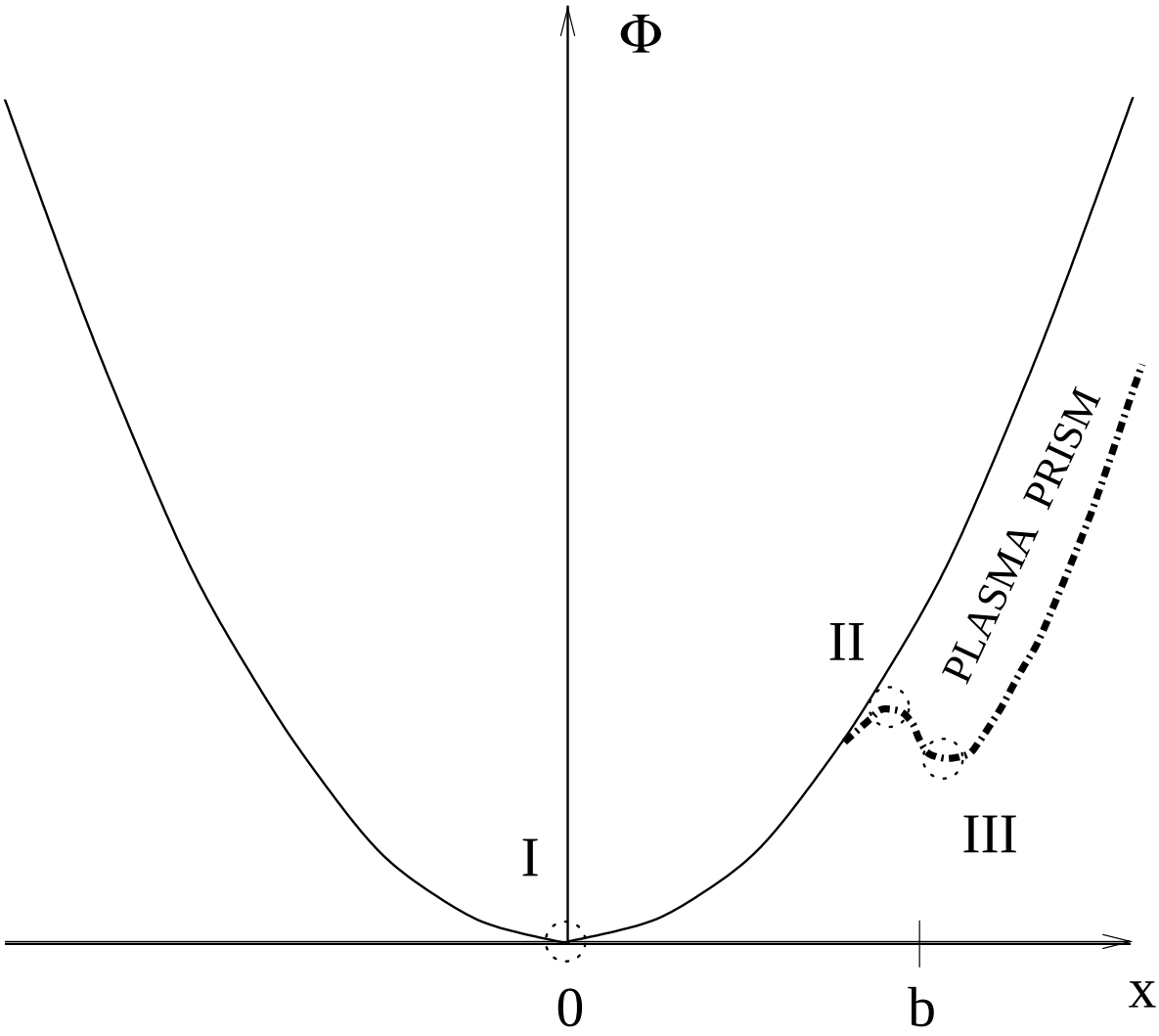

Fig. 8.— Cross section of the phase screen including a quadratic Fresnel bowl (solid) with the addition of the leading, sinusoidal edge of prism (dot-dash). Stationary phase points are interpreted as: I, old emission prior to DM jump; II, ghost emission; and III, new emission viewed through the plasma prism. As a function of time the origin of the quadratic Fresnel bowl moves to the right: toward and then into the prism.

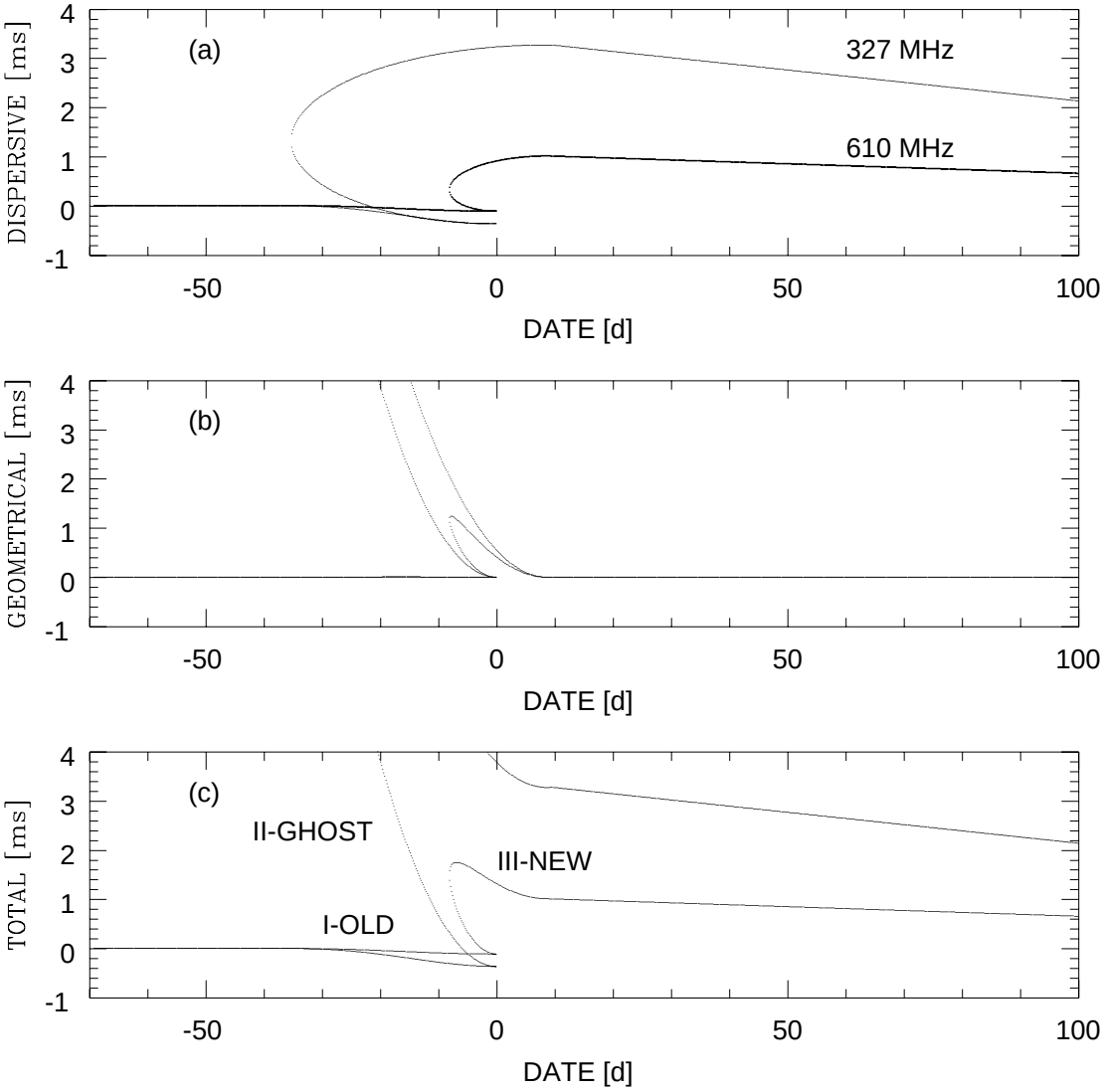

Fig. 9.— Results from a simulation of arrival times for signals passing through a plasma prism as discussed in the text. The dispersive component is shown in (a) the geometrical component in (b) and the total in (c). The outer points are at 327 MHz and inner points are at 610 MHz. In (c) the identification of simultaneous pulse locations with points of stationary phase in Figure 8 is made.

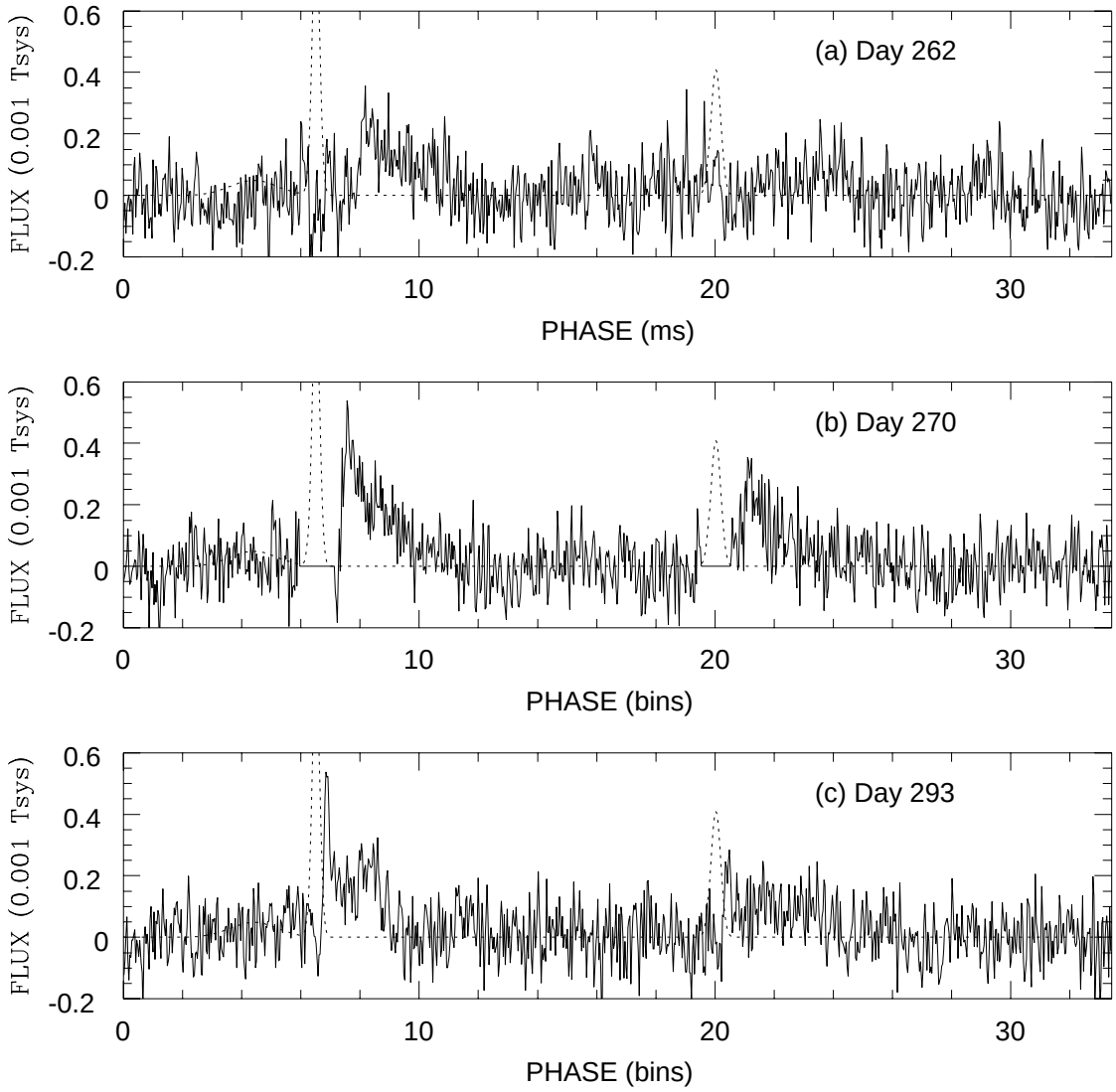

Fig. 10.— Ghost pulse components for days 262, 270 and 293 (solid). The main emission template is shown with dotted lines. The main pulse and interpulse components are distorted on day 270 and so the residuals in these regions are blanked.

Table 1. Crab Pulsar Timing Parameters

Parameter	Value
Right Ascension (J2000)[a]	05 34 31.973
Declination (J2000)[a]	22 00 52.07
Period (s)	0.033458496298951444
Period Derivative (10^{-15}s s^{-1})	420.6590250882
Second Derivative (10^{-30}s s^{-2})	-1521098.959
Epoch (MJD)	50260.00
Dispersion Measure (cm^{-3}pc)	56.791

[a]**?**)

Table 2. Crab Pulsar Profile Model [a]

Frequency (MHz)	Component	Relative Phase,$\phi_{\rm n}$ (deg)	Relative Amplitude, $A_{\rm n}$	Width, $W_{\rm n}$ (deg)
327[b]	precursor	196.5± 0.5	0.43± 0.05	16.4± 0.6
	main pulse	214.28± 0.05	1.50± 0.08	2.8± 0.1
	interpulse	0.0	1.00	3.5± 0.1
610[c]	precursor	195.0± 0.9	0.14± 0.02	12.0± 4.0
	main pulse	214.40± 0.08	2.08± 0.14	3.3± 0.3
	interpulse	0.0	1.00	4.1± 0.3

[a]Gaussian component model: $\Sigma(A_{\rm n}\sqrt{2\pi W_{\rm n}})\exp[-(\phi-\phi_{\rm n})^2/2\sigma_{\rm n}^2]$; $W_{\rm n}\equiv 2\sqrt{2\ln(2)}\sigma_{\rm n}$

[b]From low scattering days: 1995 June 23; 1997 January 12; 1999 May 28; 1999 November 28

[c]From: 1995 June 23; 1997 January 12; 1999 November 28; 1999 December 31

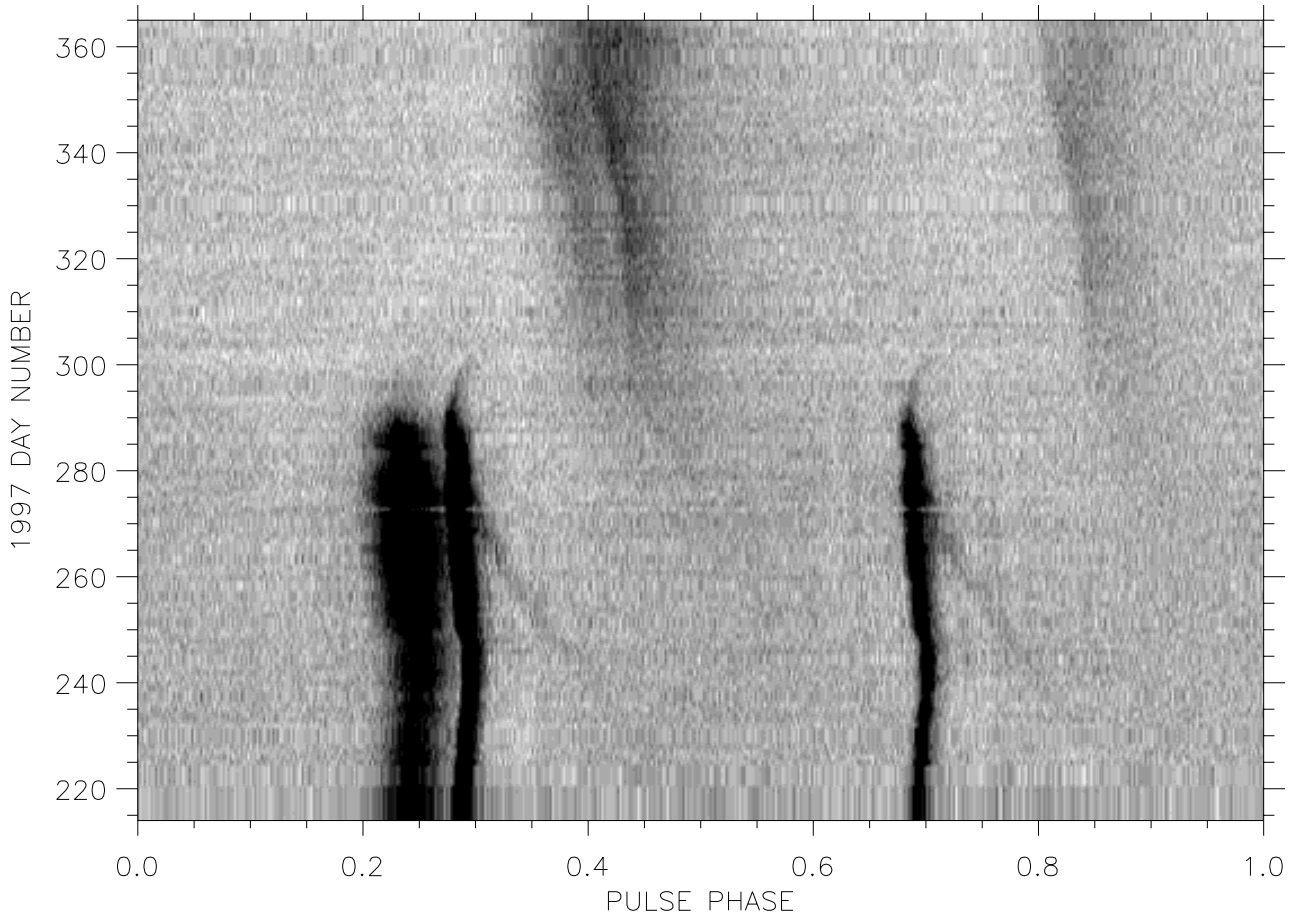
360
340
320
300
280
260
240
220
1997 DAY NUMBER
0.0
0.2
0.4
0.6
0.8
1.0
PULSE PHASE

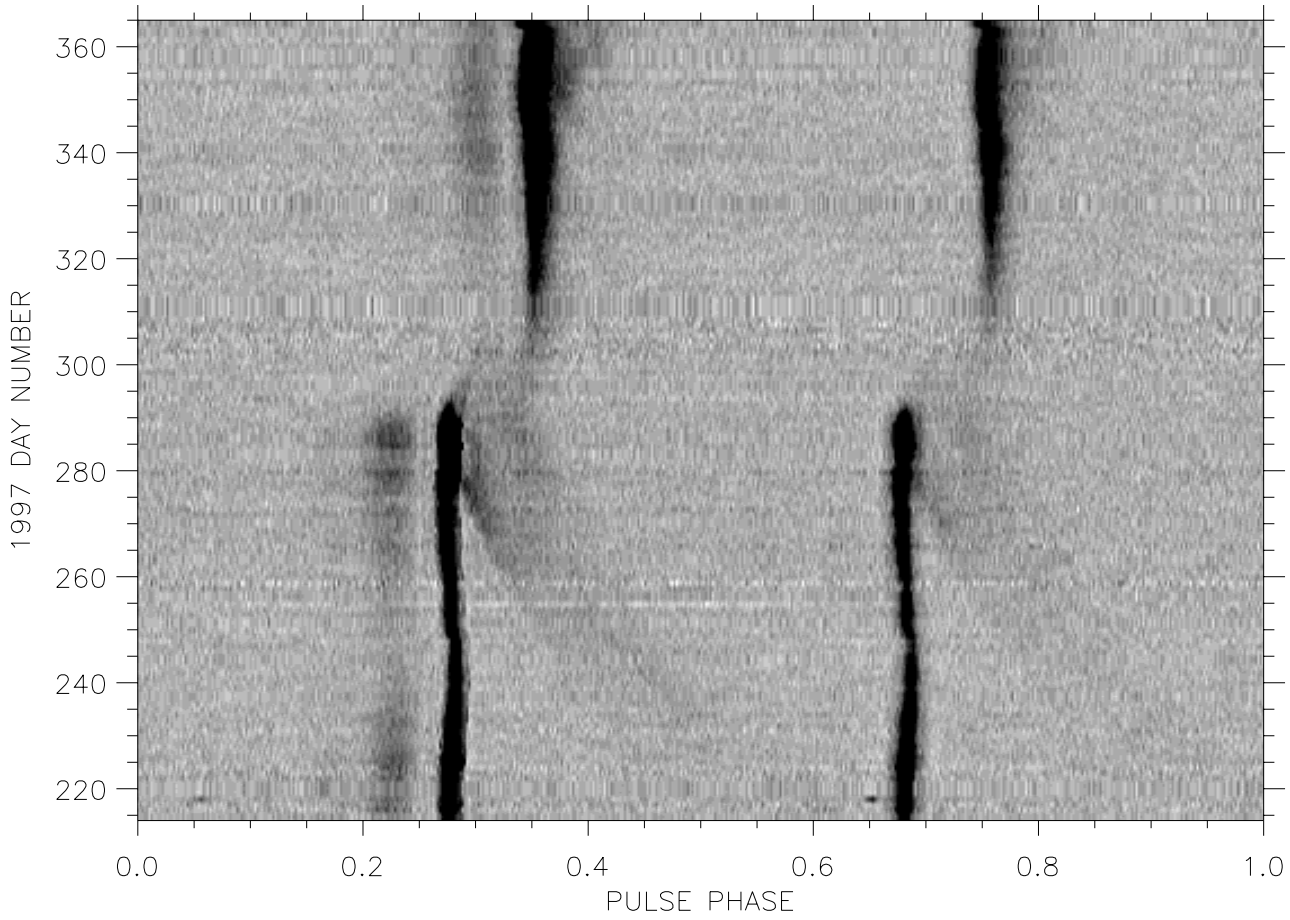
360
340
320
300
280
260
240
220
1997 DAY NUMBER
0.0
0.2
0.4
0.6
0.8
1.0
PULSE PHASE

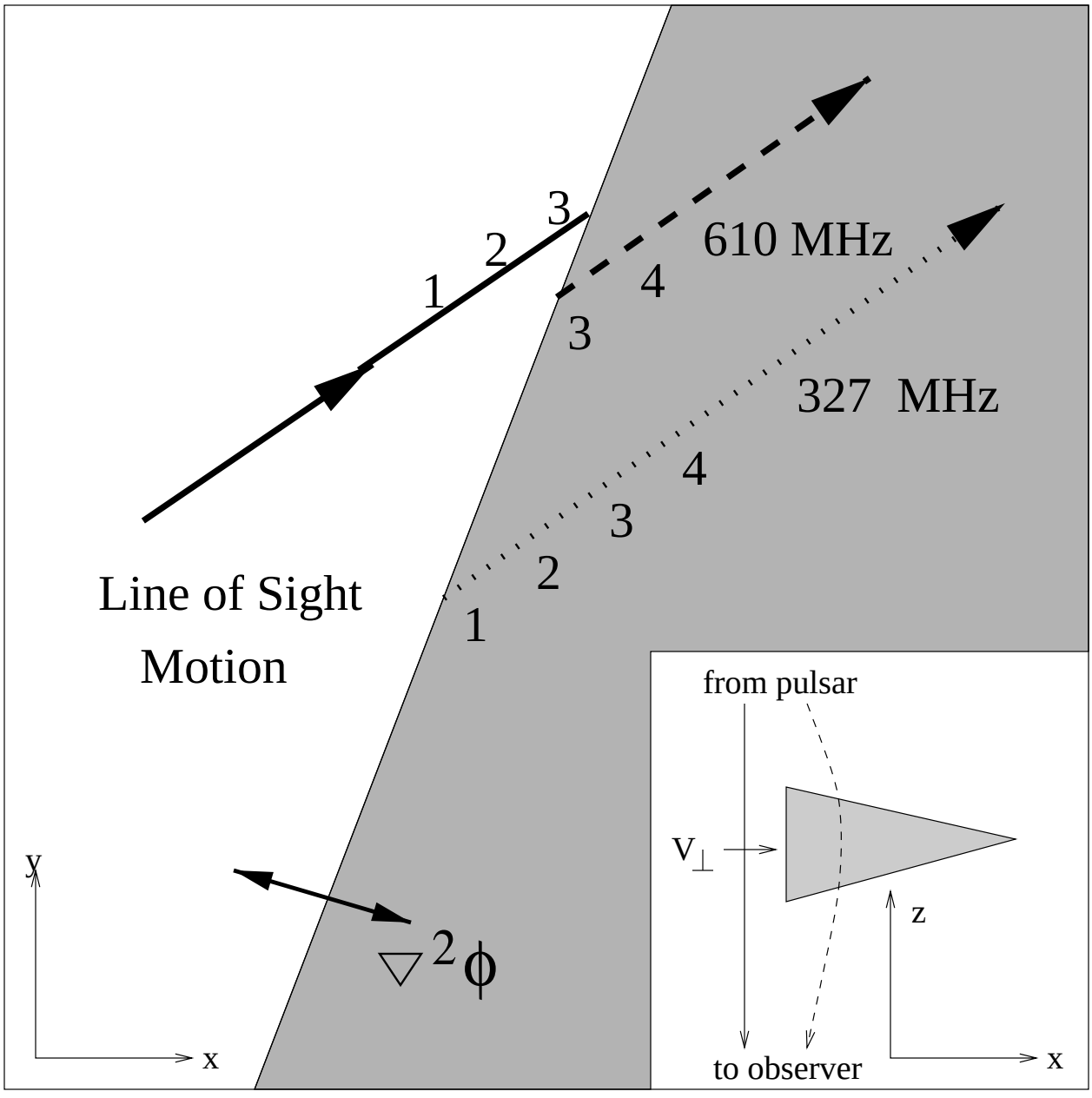
610 MHz
327 MHz
1
2
3
4
3
4
3
2
1
Line of Sight
Motion
$\nabla^2\phi$
y
x
from pulsar
$v_\perp$
z
x
to observer

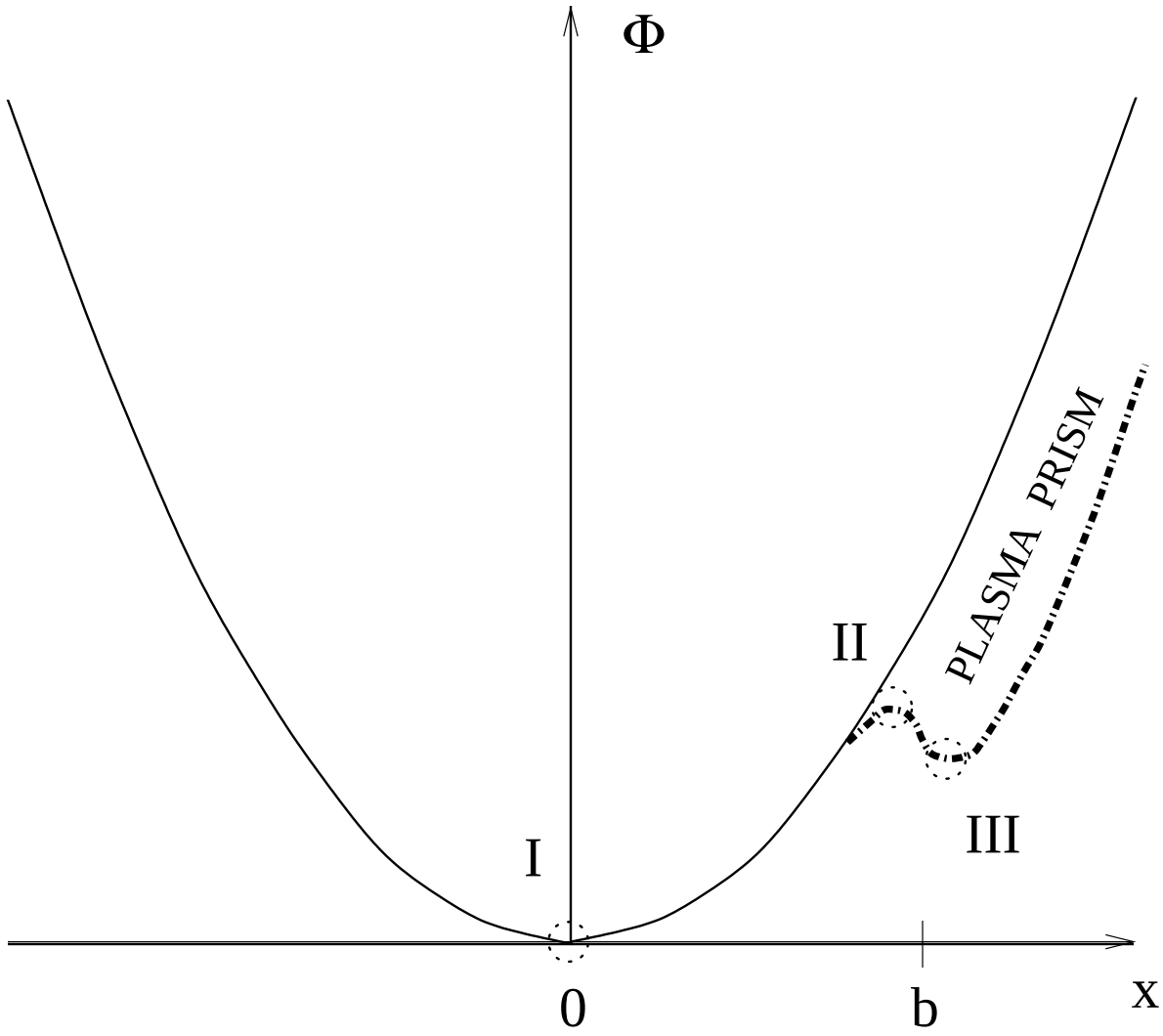
Φ
PLASMA PRISM
II
III
I
0
b
x